

The Preliminary CatWISE Catalog: Motions from *WISE* and *NEOWISE* Data

PETER R. M. EISENHARDT,¹ FEDERICO MAROCCHI,^{1,*} JOHN W. FOWLER,² AARON MEISNER,³
NELSON GARCIA,⁴ THOMAS H. JARRETT,⁵ J. DAVY KIRKPATRICK,⁴ RENATA KOONTZ,⁶
ELIJAH J. MARCHESE,⁶ S. ADAM STANFORD,⁷ DAN CASELDEN,⁸ MICHAEL C. CUSHING,⁹
ROC M. CUTRI,⁴ JACQUELINE K. FAHERTY,¹⁰ CHRISTOPHER R. GELINO,⁴ ANTHONY H. GONZALEZ,¹¹
AMANDA MAINZER,¹ BAHRAM MOBASHER,⁶ DAVID J. SCHLEGEL,¹² DANIEL STERN,¹
HARRY I. TEPLITZ,⁴ AND EDWARD L. WRIGHT¹³

¹*Jet Propulsion Laboratory, California Institute of Technology, 4800 Oak Grove Drive, M/S 169-327, Pasadena, CA 91109, USA*

²*230 Pacific St., Apt. 205, Santa Monica, CA 90405 USA*

³*National Optical Astronomy Observatory, 950 N. Cherry Ave., Tucson, AZ 85719, USA*

⁴*IPAC, Mail Code 100-22, Caltech, 1200 E. California Blvd., Pasadena, CA 91125, USA*

⁵*Department of Astronomy, University of Cape Town, Private Bag X3, Rondebosch, 7701, South Africa*

⁶*University of California, Riverside, 900 University Ave, Riverside, CA 92521*

⁷*Department of Physics, University of California Davis, One Shields Avenue, Davis, CA 95616, USA*

⁸*Backyard Worlds, Moraga, CA, USA*

⁹*Department of Physics and Astronomy, University of Toledo, 2801 West Bancroft St., Toledo, OH 43606, USA*

¹⁰*American Museum of Natural History*

¹¹*University of Florida*

¹²*Lawrence Berkeley National Laboratory, Berkeley, CA, 94720, USA*

¹³*Department of Physics and Astronomy, UCLA, 430 Portola Plaza, Box 951547, Los Angeles, CA 90095-1547, USA*

(Revised June 6, 2019)

Submitted to

Corresponding author: Peter R. M. Eisenhardt. To be submitted to the Astronomical Journal.
Peter.R.Eisenhardt@jpl.nasa.gov

ABSTRACT

The Preliminary CatWISE catalog consists of 900,849,014 sources over the entire sky selected from *WISE* and *NEOWISE* survey data at 3.4 and 4.6 μm (W1 and W2) collected from 2010 to 2016. This dataset represents four times as many exposures and spans over ten times as large a time baseline as that used for the AllWISE catalog. CatWISE adapts AllWISE software to measure the sources in co-added images created from six month subsets of these data, each representing one coverage of the inertial sky, or epoch. The catalog includes the measured motion of sources in 8 epochs over the 6 year span of the data. From comparison to *Spitzer*, the SNR 5 Vega magnitude limits are W1=17.58 and W2=16.43, vs. W1=16.90 and W2=15.95 for AllWISE. From comparison to *Gaia*, the motions are an order of magnitude more accurate than those from AllWISE. The catalog is available to the astrophysics community at <https://catwise.github.io>.

Keywords: catalogs

1. INTRODUCTION

NASA’s Wide-field Infrared Survey Explorer mission (*WISE*; Wright et al. 2010) revealed iconic objects, including the first Earth Trojan asteroid (Connors et al. 2011), the closest and coolest brown dwarfs (Luhman 2013, 2014), and the most luminous galaxy yet found in the Universe (Tsai et al. 2015). These discoveries were made using two or more infrared coverages of the sky (or epochs) obtained from January 2010 to February 2011. Each epoch typically consists of a dozen exposures per band taken within two days at a given position. The satellite was reactivated as *NEOWISE* and resumed searching for near Earth objects in December 2013 (Mainzer et al. 2014), and has continued to cover the sky every six months since then.

* NASA Postdoctoral Program Fellow

In November 2013, the AllWISE release (Cutri et al. 2013) made available to the community an atlas from coadding the two dozen exposures from the initial year of WISE surveying, and a catalog of source fluxes and positions measured from those exposures. With at least two epochs per inertial position, AllWISE also provided motion estimates, and became the definitive catalog in the WISE bandpasses. Each year, *NEOWISE* releases the individual exposures from the reactivated survey (Cutri et al. 2015), corresponding to two additional epochs. With the 2019 April 10 *NEOWISE* release, exposures from 12 epochs, each of which typically has a dozen or more exposures at a given position, are now available. Meisner et al. (2018a) used unWISE processing (Lang 2014) to produce an image atlas which combines the 2010 and 2011 data used for AllWISE with the 2013 through 2016 *NEOWISE* data. An obvious next step is to catalog the sources revealed in these combined exposures.

The unWISE catalog (Schlafly et al. 2019) uses a crowded-field point-source photometry code called “crowdsource” to do this, measuring source fluxes and positions in the coadded image, with the measurements at $3.4\text{ }\mu\text{m}$ (W1) and $4.6\text{ }\mu\text{m}$ (W2) carried out independently. In contrast, CatWISE has adapted AllWISE software to produce a full sky catalog of sources selected simultaneously in both W1 and W2, and also provides motion estimates. CatWISE sources in the Preliminary catalog were selected from the ensemble of 8 epochs of *WISE* and *NEOWISE* data from Meisner et al. (2018a, the “full coadd”), and the least-squares best-fit solution for point source flux, position and motion were determined from measurements on the individual “epoch coadd” images (Meisner et al. 2018d). Because the total time between CatWISE epochs is over 6 years, compared to a typical value of 6 months for AllWISE, the CatWISE motion estimates are far more accurate. This plus the greater depth of the CatWISE catalog relative to AllWISE are being used to extend the census of the coldest brown dwarfs in the solar neighborhood and enable definitive measurement of the form of the low-mass end of the star formation process.

In §2 of the paper we summarize relevant aspects of the *WISE* and *NEOWISE* mission phases. §3 describes the CatWISE processing steps. §4 assesses the astrometric and photometric performance of

CatWISE using comparisons to *Gaia* and *Spitzer* data. §5 provides some initial examples of science results enabled by CatWISE, and §6 provides information on accessing CatWISE data products.

2. OBSERVATIONS

WISE was launched on 2009 December 14, with its 40-cm telescope cooled to 12 K by an outer cryostat tank, and the W1 and W2 detectors operated at 32 K. The 12 and 22 μm (W3 and W4) detectors were cooled to 7.8 K by an inner cryostat tank. Both tanks were filled with frozen hydrogen. The cryostat cover was ejected and the first images obtained on 2009 December 31, and science survey data began being taken on 2010 January 7.

The *WISE* scan strategy covers the same region of inertial sky every six months. This repetition alternates between sides of the *WISE* orbit (as well as sides of the Earth’s orbit around the Sun), so the direction of the survey scans alternates between ascending and descending in ecliptic latitude. CatWISE processes ascending and descending scans separately for source measurement (§??).

The full cryogenic survey covered the sky 1.2 times, continuing until the hydrogen in the outer tank evaporated on 2010 August 6 (Figure 1). *WISE* then surveyed an additional 30% of the sky during its 3-Band (W1, W2, and W3) cryogenic phase, with the W3 detector operating at reduced sensitivity. After the cryogen in both tanks was exhausted on 2010 September 29, the post-cryogenic *NEOWISE* survey (Mainzer et al. 2011) in W1 and W2 began, as the telescope and detectors warmed to ~ 73 K. Surveying continued until 2011 February 1, completing a second pass over the sky in W1 and W2, after which the satellite was placed into hibernation. In September 2013, the spacecraft was brought out of hibernation, where it had equilibrated at ~ 200 K due to thermal radiation from the Earth, and renamed *NEOWISE*. On 2013 December 13, with the telescope and detectors passively cooled below 76 K, *NEOWISE* resumed surveying the sky every 6 months in W1 and W2 (Mainzer et al. 2014).

The Preliminary CatWISE catalog is based on the combination of W1 and W2 exposures in the two sky coverages used for the AllWISE data release (Cutri et al. 2013) and in the six sky coverages from the 2017 *NEOWISE* data release. We use MJD 55480 (2010 Oct. 11) as the dividing point between cryogenic and post-cryogenic data. The average observation date is closer to MJD 56700

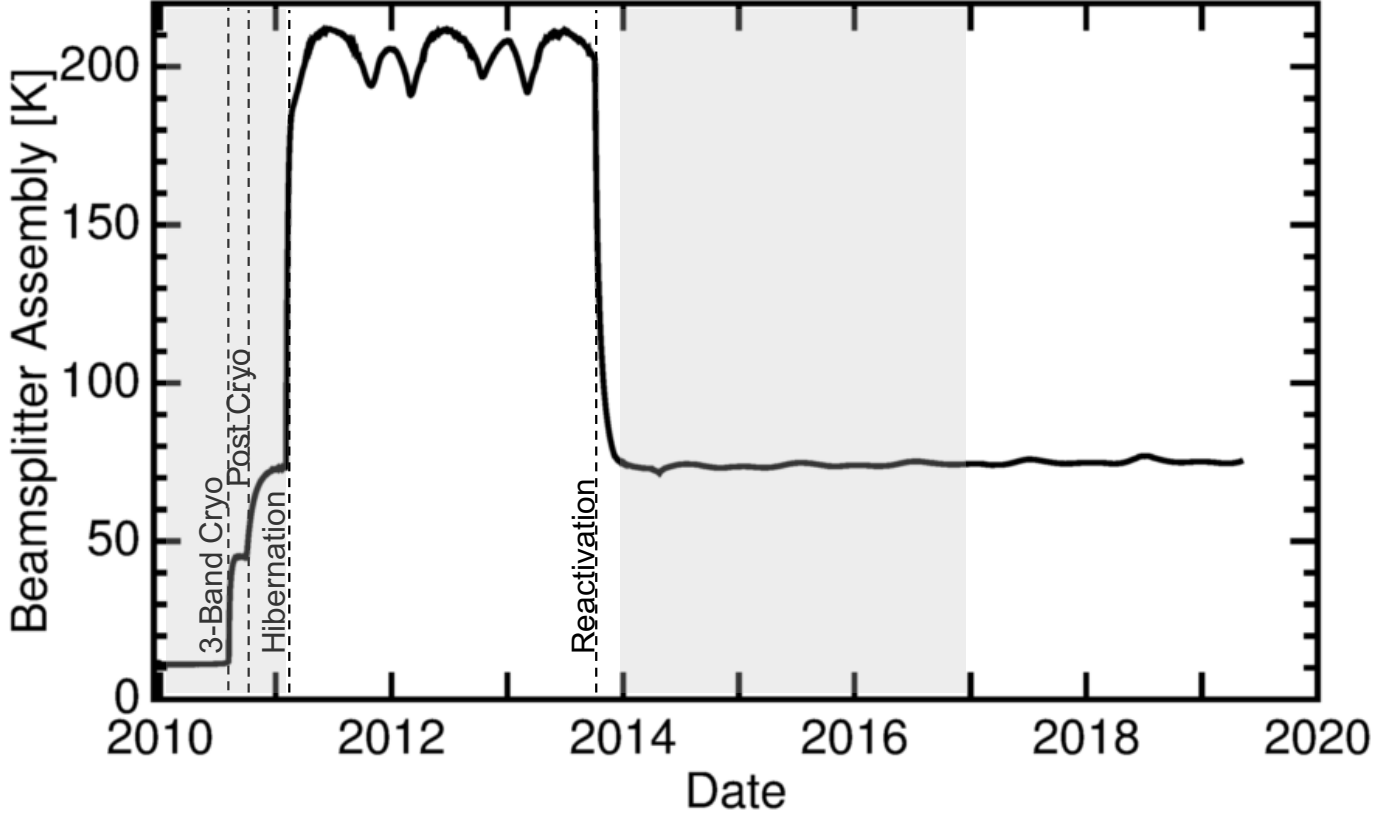


Figure 1. Temperature vs. date of the *WISE* beamsplitter assembly, which is close to the temperature of the telescope and W1 and W2 detectors. Dashed lines indicate the transitions from full cryogenic to 3-band cryogenic phases, to the post-cryogenic phase, and to the start of hibernation and reactivation. Grey shading indicates the date ranges of data used for the Preliminary CatWISE catalog. AllWISE included only the left portion of the shaded range.

(2014 Feb. 12), which we adopt as the epoch for reporting positions when solving for source motion in the Preliminary catalog. Source positions, whether incorporating source motion or not, are given in the equinox J2000 coordinate frame.

3. CATWISE PROCESSING

CatWISE adapts the AllWISE pipeline to detect and measure source fluxes in the combined WISE and NEOWISE images provided by unWISE (Lang 2014). A full description of the AllWISE pipeline is provided in Cutri et al. (2013).

CatWISE processing works in the J2000 coordinate footprint established by the WISE All-Sky Release, dividing the inertial sky into 18,240 overlapping square images (tiles), each approximately

1.56 deg on a side, aligned with the local right ascension and declination. Processing steps were carried out independently on each tile. For the Preliminary catalog, CatWISE uses the full depth unWISE coaddition of 8 epochs (Meisner et al. 2018a), and the 8 individual unWISE epoch coadds (Meisner et al. 2018d, after astrometric modifications described below). Source detection was done on the full depth coadds, and source properties determined from measurements on the epoch coadds, treating ascending and descending epochs separately for most tiles and then merging the results. Potential artifacts affecting the sources were identified, and sources with multiple measurements because they were in the tile overlap region were flagged to indicate which set of measurements should be used. Finally, sources were selected for inclusion in the catalog or reject files. We describe these steps in more detail below.

3.1. *unWISE Coadds*

The coadded images in the atlas released with the AllWISE (and All-Sky) catalogs were primarily intended to facilitate source detection, and for this reason they are convolved with the WISE PSF. The unWISE coadds retain the resolution of individual WISE exposures. To reduce differences from the AllWISE processing approach, for source detection (§3.3) in the Preliminary CatWISE catalog, we convolved the full-depth unWISE coadds (Meisner et al. 2018a) with the PSF (§3.2). For source measurement (§3.4) we used unWISE epoch coadds (Meisner et al. 2018d) without convolution.

An adjustment was made to the WCS for the pre-hibernation unWISE epoch coadds. Although all of the released individual exposures are tied to 2MASS, the individual pre-hibernation exposures released for AllWISE are not on the same astrometric system as the individual post-hibernation exposures released for *NEOWISE*. The *NEOWISE* images include corrections for the motions of the 2MASS reference stars, as does the AllWISE catalog (see §V.2.b of the AllWISE Explanatory Supplement Cutri et al. (2013)), but the released pre-hibernation images do not include those corrections. A table of corrections for these images exists, however ¹, and these corrections were applied to the

¹ http://wise2.ipac.caltech.edu/docs/doc_tree/sis/rex19

unWISE input, making the astrometric system of the pre-hibernation epoch coadds consistent with those from the post-hibernation epoch coadds.

3.2. PSF

The *WISE* and *NEOWISE* PSFs have been well characterized at the individual exposure level, but CatWISE works with co-added images rather than individual exposures, so PSFs appropriate for these co-added images are needed. The W1 and W2 PSFs vary with position in the focal plane, and changed somewhat between the cryogenic and post-cryogenic phases of the mission, particularly for W1. The PSFs are also asymmetric, with an orientation that is fixed with respect to the focal plane, but the focal plane orientation with respect to equatorial coordinates varies between exposures. The orientation also flips every six months because at a given inertial location the survey scan direction alternates between ascending and descending in ecliptic latitude. CatWISE addressed these issues as follows.

Model PSFs in a 9×9 grid over the focal plane for the cryogenic phase are provided in §IV.4.c.iii.1 of the *WISE* All-Sky Explanatory Supplement (Cutri et al. 2012), while the post-cryogenic PSFs used for *NEOWISE* are given in §IV.2.b.i of the NEOWISE Explanatory Supplement (Cutri et al. 2015). Since many focal plane positions contribute to each source in the coadded images, CatWISE averaged these model PSFs, weighted only by their partition sizes in the 9×9 array. Figure 2 (left) shows the resulting focal plane average post-cryogenic PSF model for W1. An analogous focal plane average PSF was created for W2, and for both bands using the post-cryogenic PSFs. These are referred to below as the “basic” PSFs.

The basic PSFs contain fine structure in the core that is far from being rotationally symmetric. Figure 3 shows the difference between ascending and descending orientations of the W1 post-cryogenic PSF. The bright and dark stripes in and around the core correspond to variations of more than 25% of the peak of the PSF. The center of the PSF is the most crucial region for position estimation, so getting this part of the PSF wrong has serious consequences for astrometry, and of course also photometry.

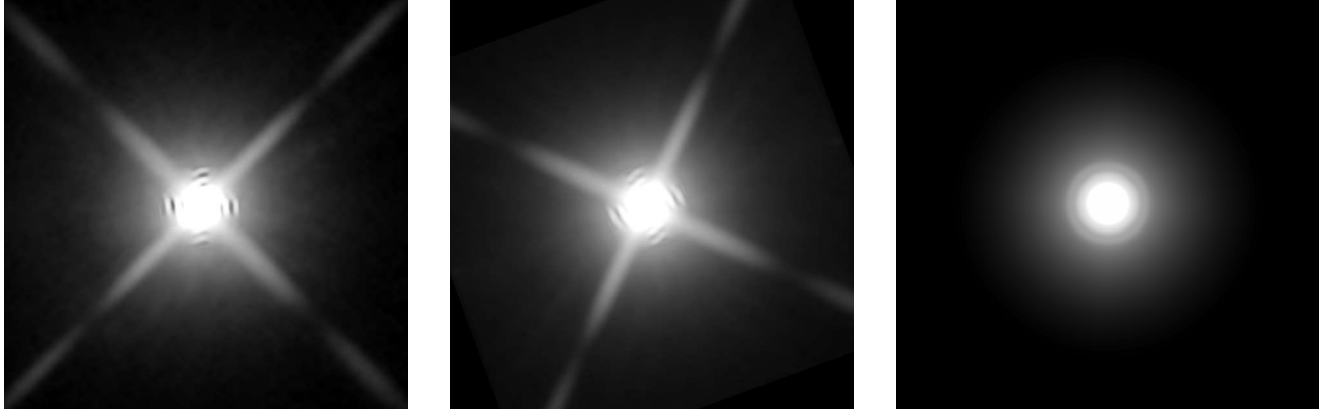


Figure 2. Left: The “basic” (averaged over focal plane position) post-cryogenic PSF model for W1. The grey scale uses a log stretch from 1% to 99% of the peak value. The model extends to $\pm 110''$. **Center:** The ascending scan W1 PSF for tile 1497p015 after averaging over cryogenic and post-cryogenic epochs, and a PA range from 199.93° - 200.56° . **Right:** The W1 PSF averaged over all scans for tile 0890m667, which includes the south ecliptic pole and all PAs.

The structure revealed here has no impact on the measurements carried out by the *WISE* and *NEOWISE* projects, because those measurements are made on individual exposures. The PSF structure is captured in the models, and the PSF orientation is always the same in the focal plane. But this is not the case for CatWISE, which uses coadds in place of individual *WISE* exposures. The coadded image tile orientation is aligned with the local equatorial coordinates. Therefore CatWISE rotated the basic PSFs by an appropriate set of position angles (PAs) between focal plane and equatorial coordinates for each image tile.

The coadded images were assembled from individual exposures with a range of PA values, so histograms of exposure PA values were constructed for each tile, using a bin width of 0.1 degrees. Separate histograms were constructed for ascending vs. descending and cryogenic vs. post-cryogenic exposures. The basic PSF was rotated by each PA bin center value and these rotated PSFs averaged together with weights equal to the histogram bin count. Those averages were then combined for each tile with weights given by the number of corresponding cryogenic and post-cryogenic exposures to make ascending and descending PSFs for each tile.

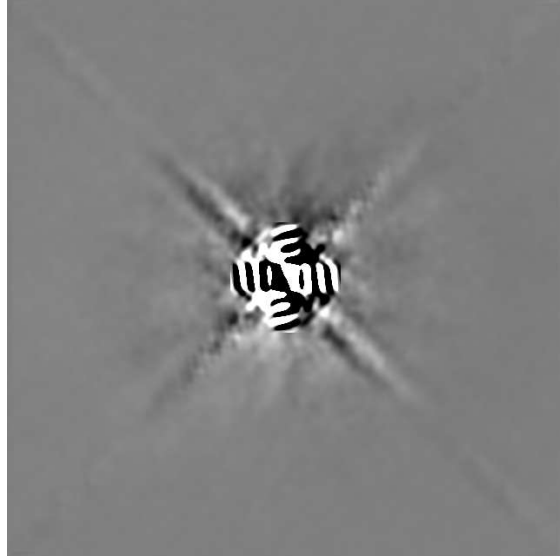


Figure 3. Difference image of W1 post-cryogenic PSFs in ascending vs. descending scans.

Tiles in the vicinity of the ecliptic poles have large PA ranges, and so the tile PSF becomes very smeared (see Figure 2 (right)). For the 50 tiles nearest the ecliptic poles, the ascending and descending PSFs were averaged together weighted by the number of ascending and descending exposures. For all tiles, a down-sampled central cutout of the average of the ascending and descending PSFs for each tile was used for the detection step.

3.3. *Detection*

Source detection for the Preliminary CatWISE catalog was done simultaneously in W1 and W2 with the Multiband Detection (MDET) software used in the WISE pipeline (Marsh & Jarrett 2012). The Image Co-addition with Optional Resolution Enhancement (ICORE) software (Masci 2013) was used to resample the 2048×2048 $2.^{\circ}75$ pixel NEO3 unWISE coadds to the 4095×4095 $1.^{\circ}375$ pixel detection image format used for WISE, using a PSF appropriate for each tile and band (§3.2) as the interpolation kernel. The PSF interpolation kernel smooths the images, providing a matched filter for optimal detection of isolated point sources.

Additional observations should improve the reliability of low SNR detections. AllWISE, with two sky coverages, selected a minimum SNR threshold of 2.4, compared to 3.5 used for the single

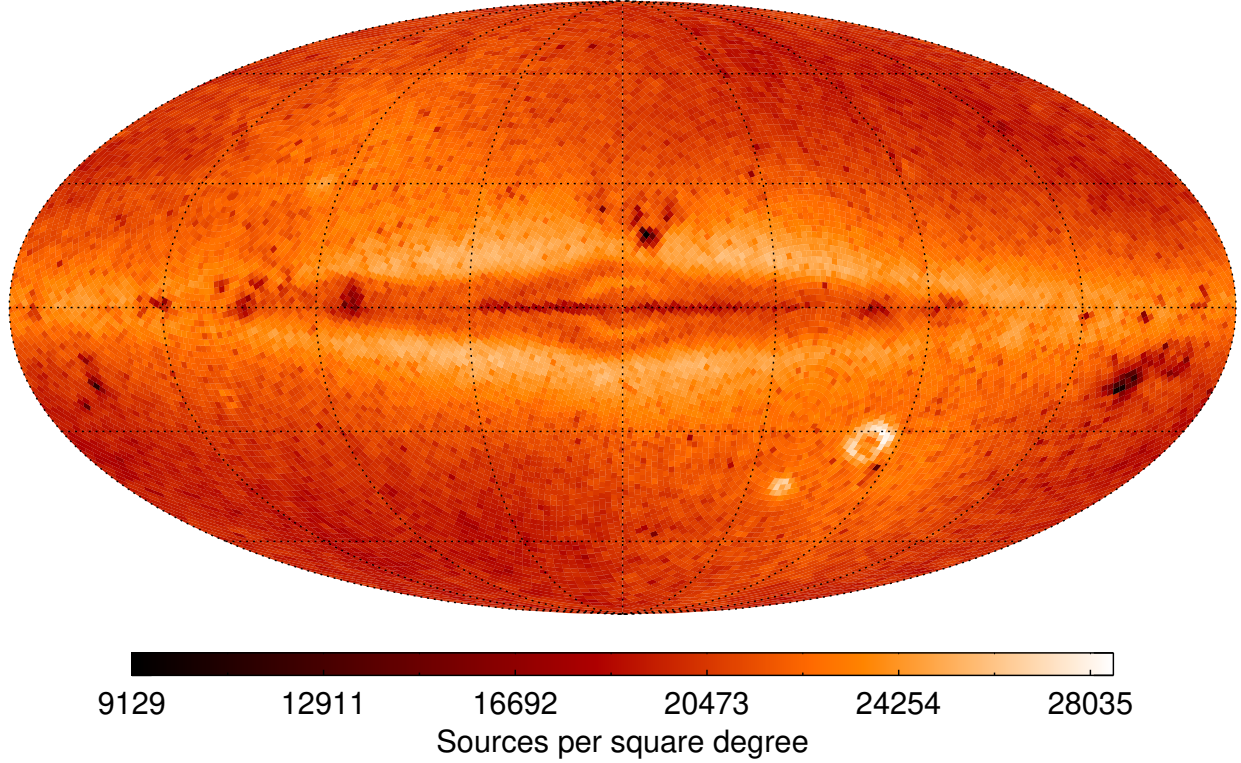


Figure 4. Map of CatWISE catalog source density in galactic coordinates.

covewrage WISE All-Sky Release. For CatWISE we estimated the SNR corresponding to a source reliability of 50% based on comparison to deeper *Spitzer* data from the SERVS ([Mauduit et al. 2012](#)) and S-COSMOS ([Sanders et al. 2007](#)) programs. This SNR varied from 1.7 in the COSMOS field to 2.6 in the Lockman Hole, and a threshold of 1.8 was selected for the Preliminary catalog.

At the high source densities typical for CatWISE in coadds of ~ 100 or more individual WISE exposures, this matched filter detection methodology yields an asymptotic number of $\sim 60,000$ detected sources per tile for the Preliminary catalog (or $\sim 25,000 \text{ deg}^{-2}$, Figure 4) and hence becomes incomplete, particularly in W1. Schlafly et al. (2019) present an alternative approach (“crowdsouce”) which results in higher detected source densities, but does not provide motion estimates.

3.4. Source Measurement

Source photometry, astrometry, and motion estimation for CatWISE use an adapted version of the WPHOT software developed for the AllWISE pipeline. WPHOT carries out point-source extraction, solving for both photometry and astrometry simultaneously. For AllWISE, source positions detected in each coadded tile image were propagated to individual exposures, and the least-square best-fit to the PSF for source position and flux were solved for. A linear motion was also solved for, based on the observation time of the images.

CatWISE did not have the computational resources to perform the source fitting on all of the many hundreds of individual exposures that contribute to a coadded tile image. Because the 12 exposures for a given inertial position in each sky coverage are obtained within less than two days, the motions of sources beyond the solar system can be assumed to be fixed for each sky coverage (or epoch). Therefore CatWISE ran WPHOT treating unWISE epoch coadd images as the individual images.

The other significant modification to the AllWISE WPHOT process implemented by CatWISE addressed the alternating scan direction of each epoch and hence varying PSF orientation. WPHOT was not designed to use a time-dependent PSF, but with 8 or more epoch coadd images per position, CatWISE elected to measure source properties with WPHOT separately for the groups of four or more epoch coadds in each of the two scan directions, and then merge the two results. This methodology, which we refer to as “option 1” below, was used for all but the 50 tiles closest to the ecliptic poles. For those 50 tiles, an average PSF of was used for all epoch coadds, and they were processed together with WPHOT. We refer to this methodology as ‘option 0’ below.

WPHOT performs PSF-fit photometry and astrometry assuming sources are inertially fixed (the “stationary fit”), and also searches for a solution assuming a linear motion with time (the “motion fit”). The χ^2 minimization fit can be performed at any location in the flux image. The goal of astrometry is to find the location at which χ^2 is at the bottom of a local minimum.

The stationary fit treats χ^2 as a function defined on a two-dimensional space: right ascension (α) and declination (δ). As one moves around in the space, χ^2 decreases and increases as the local flux distribution appears more or less like a point source. In the vicinity of a real point source, χ^2 tends

to be concave, although with some noise fluctuations. At any point, both χ^2 and its gradient can be calculated. The astrometry solution is found using the gradient descent method, by searching along the opposite direction of the gradient vector until the gradient flattens out and the local minimum has been found. The (α, δ) where χ^2 is estimated to be minimal is the position assigned to the source, and the scale factor on the PSF that minimizes χ^2 there is the flux estimate. The value of χ^2 is recorded, as are the individual χ^2 for the W1 and W2 flux fits. Standard Gaussian error analysis provides uncertainties for (α, δ) and flux. The error model includes both PSF error and image flux error, and is discussed further in 3.4.1. More details on WPHOT are given in §IV.4.c.iii of the *WISE* All-Sky Explanatory Supplement ([Cutri et al. 2012](#)).

The motion fit treats χ^2 as a function defined on a four-dimensional space, $(\alpha, \delta, \mu_\alpha, \mu_\delta)$, where μ_α and μ_δ are the angular motions in (α, δ) . The model used for the motion solution replaces the single location of the stationary solution with locations along a linear function of time. The slopes of this line in the (α, δ) directions are the motions (μ_α, μ_δ) . When the motion fit is based on both ascending and descending epochs, the motions will include parallax effects (see [Kirkpatrick et al. 2014](#)), and so they are not true proper motions. However, for nearly all tiles, CatWISE processed ascending and descending scans separately, separating the observations into opposite elongations, so that the measured motions are true proper motions.

3.4.1. Uncertainties

For uncertainties, the “std” unWISE images were used, which are the sample standard deviation at each pixel of the individual WISE exposures divided by $\sqrt{N - 1}$, where N is the number of exposures. Reduced chi-square values from the CatWISE PSF fitting showed that the uncertainties needed adjustment.

The adjustments were made to the PSF and image uncertainties, with the goal of making the PSF-fit reduced chi-square values come close to 1.0 for non-saturating sources. The PSF uncertainties were scaled down by 0.9 in W1 and 0.64 in W2 based on bright star reduced chi-squared values. Cryogenic PSF uncertainties for W1 were scaled down further by 0.58. Based on faint star reduced chi-squared values, the image uncertainties were scaled up by 1.4 in W1 and 1.15 in W2, and those for

pre-hibernation epochs were scaled up further by 1.1 in W1 and 1.05 in W2. In addition, a minimum value of 1 DN in W1 and 10 DN in W2 was imposed on the image uncertainties.

The uncertainties for the 50 tiles near the ecliptic poles, which used averages of ascending and descending PSFs (3.2) had somewhat different adjustments. For these tiles the PSF uncertainties were scaled up by 1.3 in W1, with no further adjustment for cryogenic values, and were left unchanged for W2. The image uncertainties were scaled up by 1.75 in W1 and 1.25 in W2, and those for pre-hibernation epochs were scaled up further by 1.1 in W1 and 1.05 in W2. A minimum value of 1 DN in W1 and 5 DN in W2 was imposed on the image uncertainties.

3.4.2. *Merging Measurements from Ascending and Descending Scans*

As noted earlier, for nearly all tiles two independent measurements were made, one extracted from epoch coadds constructed from ascending scans and one from descending-scan epochs. These were merged into a single source list as follows.

Each source has an identifier (“mdetID”) corresponding to an entry in the detected source list (3.3), and this was used to match ascending and descending measurements of the same source. The ascending and descending sources were almost in perfect one-to-one correspondence, but a small number of mismatches occurred because of active deblending in WPHOT. Active deblending inserts a new source (not from the detection program) into the fitting region if the chi-square value exceeds a threshold and is reduced by a minimum required amount by the insertion. Full details may be found in §IV.4.c of the *WISE* All-Sky Explanatory Supplement. Active deblending may proceed differently in the ascending and descending data. Actively deblended sources have the same mdetID, so when that is not unique, a nearest-match criterion is applied. The number of ascending sources may not equal the number of descending sources, so that some sources are left over and discarded, leaving a one-to-one association list.

Corresponding parameters for each matched ascending-descending source pair were combined when the ascending and descending apparitions have non-null values, otherwise the single non-null values (if any) were retained. Aperture magnitudes are computed from the same full-depth coadd in Asce and Desc, differing only slightly in the position of the aperture centers. These magnitudes and

their uncertainties are simply averaged without weighting. Positions were averaged using inverse-covariance weighting, with the averaging done in a local Cartesian projection consistent with the uncertainty representation. Additional details are provided in Appendix A. PSF-fit photometry was combined by averaging the flux values using inverse-variance weighting. This yields refined flux values and reduced uncertainties that are used to recompute the magnitudes, magnitude uncertainties, and signal-to-noise ratios.

3.5. *Artifact Flagging*

Bright stars create a variety of scattered light effects and electronic-charge issues that require special handling by the software. These effects include scattered light halos, diffraction spikes, glints from off-frame bright stars, optical ghosting from internal reflections within the optical system, and charge persistence on the arrays. These can create false detections, hereafter called artifacts, or can contaminate detections of real, astrophysical sources. The goal of artifact flagging is to label spurious or affected sources so that the user can easily create source lists for which most of these problems are eliminated.

The Preliminary CatWISE catalog employs two types of artifact flagging. One is the *cc_flags* values copied directly from AllWISE processing. If a source was found in either the AllWISE catalog or reject table within 2 $''$.75 of a CatWISE source, its *cc_flag* was included in the entry for the CatWISE source; if no AllWISE source was found within this radius, then *cc_flags* contains a null value. These *cc_flags* values indicate whether a source is thought to be dominated by a real artifact (encoded as an upper-case letter) or a real source contaminated by an artifact (encoded as a lower-case letter). Each band is flagged separately, and since AllWISE processing included data in all four WISE bands the *cc_flags* value is a four-character string. The possibilities are “O” for no artifact or contamination, “D” or “d” for a diffraction spike, “H” or “h” for a scattered light halo, “O” or “o” for an optical ghost, or “P” or “p” for charge persistence. Note that the *cc_flags* field conveys only the main features of the full artifact flag information contained in the AllWISE *w1_c_map*, *w1_c_mapstr*, *w2_c_map*, and *w2_c_mapstr* fields, which are also provided in the CatWISE source entry. A more detailed description can be found in § IV.4.g of the *WISE* All-Sky Explanatory Supplement ([Cutri et al. 2011](#))

al. 2012). For a CatWISE source having multiple AllWISE sources within the $2.^{\circ}75$ radius, the most pessimistic value per band is retained, as described in §3.5.1.

The second type of artifact flags are called *ab_flags*, which were determined for every CatWISE source. The *ab_flags* do not attempt to distinguish between an outright artifact and a real astrophysical source that suffers from some level of artifact contamination. However, we have adjusted the flagging (§ 3.5.3) so that only egregious artifacts more likely to be spurious detections are flagged. By analogy with *cc_flags*, the *ab_flags* thus contain only upper-case letters “D”, “H”, “O”, or “P” or the value “0”. Furthermore, because the CatWISE data deal only with W1 and W2 data, the *ab_flags* values are only two characters long. Additional details are given in § 3.5.2.

These *cc_flags* and *ab_flags* values should be regarded as two different yet complementary methods for tagging sources of special concern to the user. As described in § IV.4.g of the *WISE* All-Sky Explanatory Supplement (Cutri et al. 2012), the *cc_flags* are known to overflag; their purpose is to produce a reliable catalog of source extractions free of contamination by artifacts, but they do so at the expense of completeness. To provide a complement to the *cc_flags*, the *ab_flags* are used to tag only the most egregious artifacts, thereby emphasizing completeness, albeit at the expense of reliability. Users of the CatWISE data products can thus query against these two sets of artifact flags to best fit their needs.

3.5.1. Setting the *cc_flags* Values When There are Multiple Matches

The values of *cc_flags* are taken directly from a join of the AllWISE Point Source Catalog and Reject Table. When more than one of these AllWISE sources matches to within $2.^{\circ}75$ of a CatWISE source, the band-by-band *cc_flags* value of the CatWISE source is determined as follows. If there is an upper-case letter for any matching source, it takes precedence over any lower-case letter. The letter “D” is the highest priority followed, in order, by “P”, “H”, and “O”. If there are no upper-case letters for any matching source, lower-case letters have the next highest priority, in the same order (“d”, “p”, “h”, and “o”). If all matching sources have a value of “0” in that band, then “0” is used.

3.5.2. Translating the *unWISE* Bit Mask Values to *ab_flags*

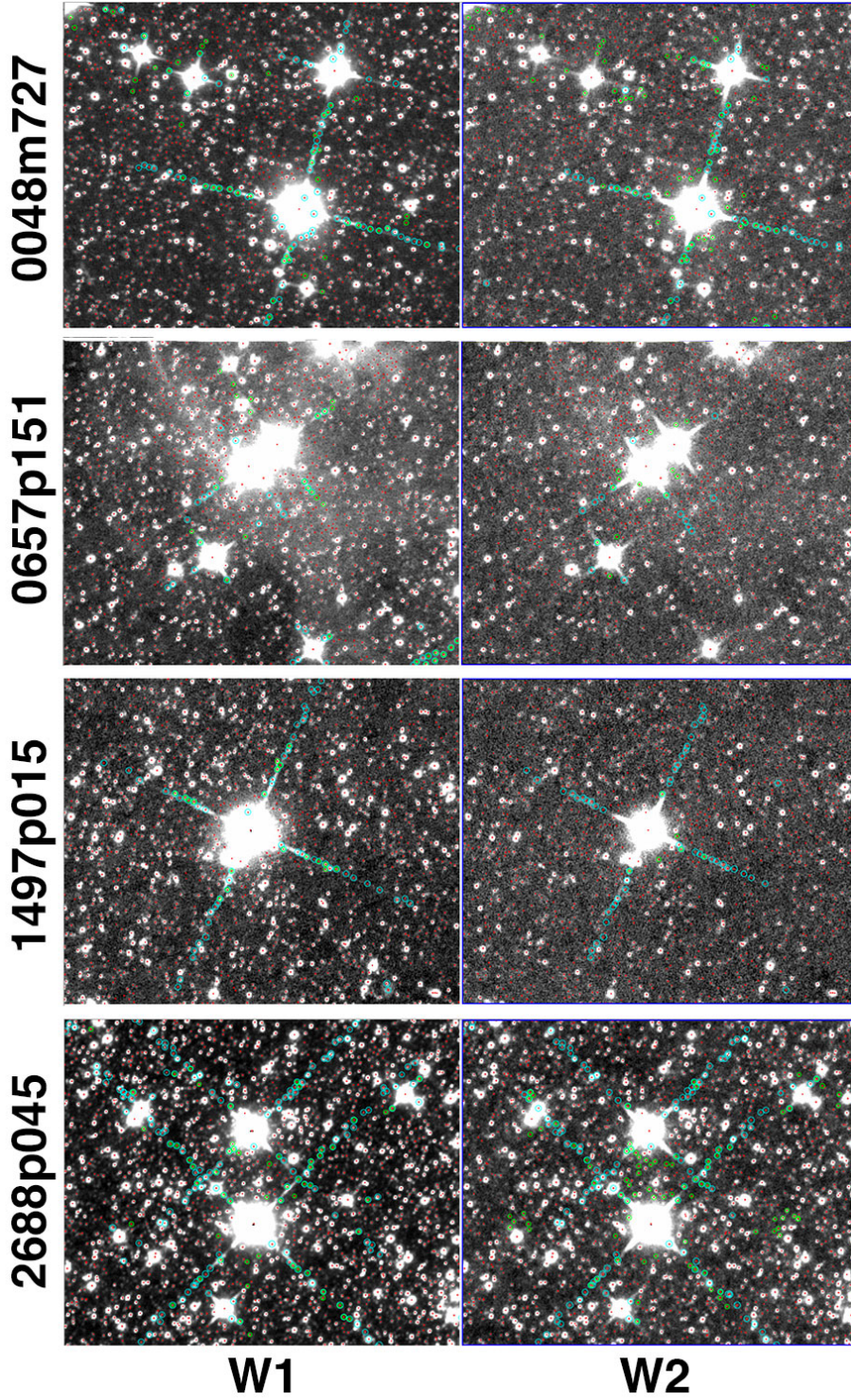


Figure 3. Each row shows W1 (left) and W2 (right) cutouts of tiles whose names are given along the far left. Detected CatWISE sources are shown by the red markers. Sources with upper-case *cc_flags* are circled in green and sources marked as artifacts by *ab_flags* are circled in cyan. Zoom in for details.

The unWISE bit mask values at the (x,y) pixel location of the source are used to set the value of *ab_flags*, as shown in Table 1, where we use the prefix “b” to indicate specific unWISE mask bits in column 3. A full description of the native unWISE mask bit meanings is available through the unWISE Catalog data release website². Note that the checks against b21 and b22 are to ensure the the bright star itself is not flagged as either a diffraction spike or scattered light halo.

Table 1. Logic Used in Converting unWISE Bitmask Values to *ab_flags* Values

Value	Band	Logic
(1)	(2)	(3)
“D”	W1	b0 or b1 or b7 or b27 or b29 but only if not b21
...	W2	b2 or b3 or b8 or b28 or b30 but only if not b22
“H”	W1	b23 but only if not b21
...	W2	b24 but only if not b22
“O”	W1	b25 or b26
...	W2	b11 or b12
“P”	W1	b13 or b14 or b17 or b18
...	W2	b15 or b16 or b19 or b20

In addition to the *ab_flags* field, the CatWISE catalog contains more fields with detailed artifact flag information (*w1_ab_map*, *w1_ab_mapstr*, *w2_ab_map*, and *w2_ab_mapstr*) for each source.

3.5.3. Adjusting the *ab_flags* Values

For the *ab_flags*, we performed by-eye checks on selected tiles to make sure that the extent of the flagging matched expectations. These included tiles at range of Galactic latitudes. Several

² http://catalog.unwise.me/files/unwise_bitmask_writeup-03Dec2018.pdf, see Table 1.

iterations were performed, primarily to tweak the extent of the halo flagging, before values were finalized. Figure 3 shows examples of these final checks in tiles containing 47 Tucanae (0048m727, $b = -44^\circ$), a portion of the Hyades (0657p151, $b = -24^\circ$), the COSMOS field (1497p015, $b = +41^\circ$), and Barnard’s Star (2688p045, $b = +15^\circ$). Note that the upper-case *cc_flags* slightly overflag, as designed, particularly in scattered light halos.

3.6. Primary Flagging

WISE tiles, and, therefore, un*WISE* coadds, overlap each other by $180''$ on the equator. As a result, sources appearing near the edge of a tile will also be measured in neighboring tiles. To remove these duplicate measurements we adopted a pure geometric approach, equivalent to that adopted in Schlafly et al. (2019). For each source in a tile, its coordinates were used to calculate the minimum distance to the edge of the tile. The same coordinates were used to calculate the minimum distance to the edge for all neighboring tiles, and the source was flagged as primary if these other minimum distances are all smaller.

3.7. The Preliminary CatWISE Catalog

Preliminary CatWISE catalog sources are required to:

- 1) be “primary” in their tile (i.e. be from the tile where that source is furthest from the tile edge) and
- 2a) have W1 SNR ≥ 5 with no identified artifacts (a value of 0 for the “ab_flags” in the W1 part (left character) of column 178)
- or
- 2b) have W2 SNR ≥ 5 with no identified artifacts (a value of 0 for the “ab_flags” in the W2 part (right character) of column 178).

There are 900,849,014 sources that meet these criteria. The 167,831,546 sources that fail to meet these criteria go into the reject file for their tile. Reject files typically contain 8,000 sources, although near the celestial poles they can contain over 30,000 sources due to large tile overlap. There are 186 formatted columns of information about each catalog source. Reject files have one additional column,

indicating if the source is primary in its tile. Additional information about most of the columns is available in the AllWISE Explanatory Supplement. Information regarding access to the catalog is provided in § 6.

4. PERFORMANCE CHARACTERIZATION

The greatest potential for improvement of the Preliminary CatWISE catalog over existing catalogs is in providing more accurate motion measurements, due to the much longer time baseline compared to AllWISE. Hence characterization has focused on astrometric properties of the Preliminary catalog. Photometric depth is also improved due to the four times larger number of exposures than AllWISE. Characterization has emphasized comparison to external truth sets, using *Spitzer* for photometric comparisons including completeness and reliability, and *Gaia* for astrometric comparisons. We begin with the photometric assessments.

4.1. Photometric properties

The COSMOS field is an important benchmark for assessing CatWISE performance, because it has been intensively observed, is near the ecliptic ($\beta = -11$ deg), and is at fairly high galactic latitude ($b = 41$ deg). The ecliptic has the highest zodiacal emission and lowest survey coverage from *WISE*, providing a representative base for performance estimates. In contrast, confusion effects are reduced by the high galactic latitude.

Figure 5 compares CatWISE Preliminary catalog PSF-fitting photometry to $2''.9$ radius aperture photometry from the *Spitzer* S-COSMOS program (Sanders et al. 2007). These observations were obtained using longer integration times (20 minutes vs. 12 minutes) and a larger telescope (85 cm vs. 40 cm) with better image quality ($2''$ vs. $6''$) and hence are much deeper than CatWISE. The closest CatWISE source within $2''.75$ was taken as the match to the S-COSMOS source. Because the CatWISE photometry is point source fitting, S-COSMOS sources were required to have $< 10\%$ flux increase between the $1''.9$ and $2''.9$ radius apertures. In addition, because the W1 band is significantly bluer than the [3.6] band, S-COSMOS sources at [3.6] were required to have $-0.1 \leq [3.6] - [4.5] \leq 0$ (see § of the All-Sky Explanatory Supplement).

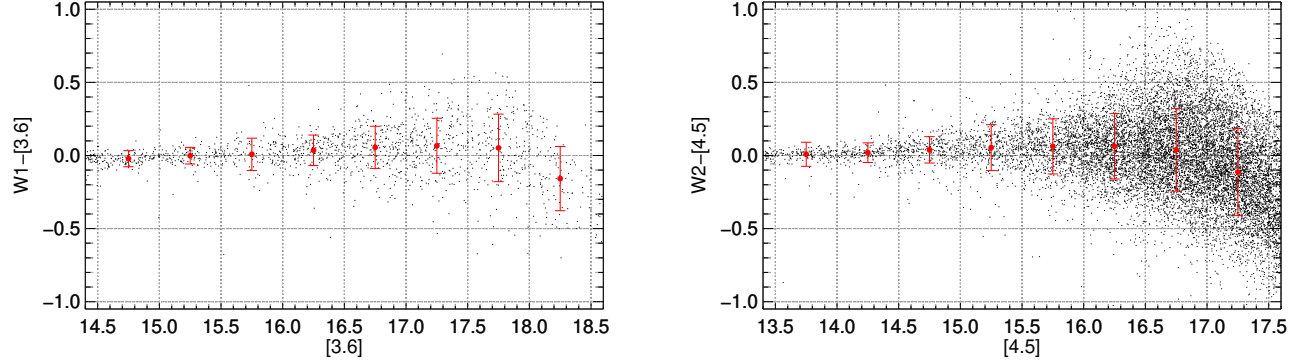


Figure 5. Comparison of CatWISE photometry to *Spitzer* photometry for COSMOS. **Left:** Difference between CatWISE W1 PSF and *Spitzer* S-COSMOS 2.9'' radius aperture photometry at [3.6], for sources with $-0.1 < [3.6] - [4.5] < 0$ and $< 10\%$ flux increase from the 1.9'' to 2.9'' aperture. Mean differences and standard deviations in 0.5 mag bins are shown by the red points and error bars. **Right:** The analogous comparison for CatWISE W2 and *Spitzer* [4.5] photometry, but without the restriction on *Spitzer* source color.

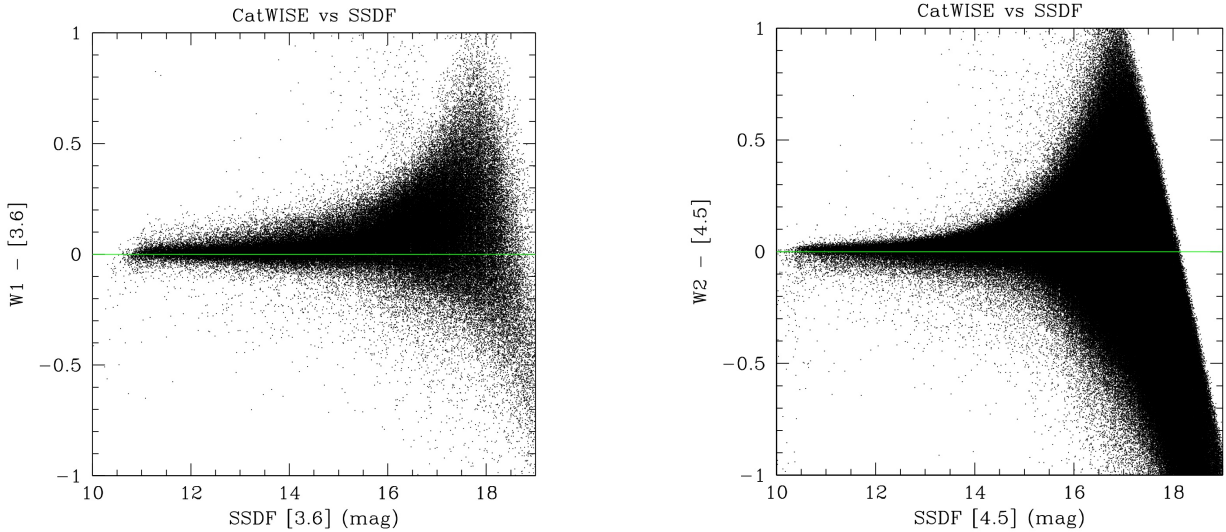


Figure 6. Comparison of CatWISE photometry to *Spitzer* photometry for SSDF.

4.2. Astrometric properties

We compared the astrometric performance of Option 1 and Option 0 on a set of 19 known ultracool dwarfs, chosen from the literature. Our test set included extremely cold, very fast moving objects (e.g. WISE J085510.83–071442.5, $\mu_{\text{tot}} \sim 8 \text{ arcsec yr}^{-1}$; Luhman 2014), as well as warmer, slower

M dwarfs (e.g. WISE J072003.20084651.2, $\mu_{\text{tot}} \sim 0.12 \text{ arcsec yr}^{-1}$; Scholz 2014). Option 1 proved superior, delivering good motion measurements for 17 out of the 19 test objects, while option 0 only recovered 13 out of the 19 test objects, with a clear drop in performance for objects with $\mu_{\text{tot}} \gtrsim 2.5 \text{ arcsec yr}^{-1}$ – only one out of the five fastest moving objects in our test sample is correctly measured by option 0, while option 1 measures four out of these five.

We note that the two objects that our pipeline is unable to correctly measure – WISE J163940.83-684738.6 and WISEPC J205628.90+145953.3 – are missed at the detection stage (§ 3.3) because they are partly blended with brighter nearby sources. These two sources were recovered when the detection step was run without the PSF filter, yielding reasonable motions, but they are not present in the Preliminary CatWISE catalog.

We tested the astrometric performance of CatWISE against *Gaia* DR2 (Gaia Collaboration et al. 2018; Lindegren et al. 2018). We chose a test set of 141 tiles, sampling a wide range of Galactic latitude (b), source density, and ecliptic latitude (β). Table 2 lists a subset of 7 out of the 141 tiles used, with their relevant properties. These 7 were chosen to sample the full b range from the South Galactic Pole to the Galactic Center, along the $l = 0^\circ$ meridian, plus the north Ecliptic pole, the South Ecliptic pole, and the tile containing the COSMOS field. Figure 7–9 shows the position and motion precision. For the comparison, we cross-matched CatWISE to *Gaia* using a two-step matching. First, we searched for *Gaia* counterparts to CatWISE sources using a broad $20''$ matching radius, and retained all matches. Then, we used *Gaia* astrometry to move the *Gaia* putative counterparts to the CatWISE epoch, and repeated the match with a narrower $2.75''$ radius (corresponding to 1 pixel in the unWISE coadds), retaining only the closest *Gaia* source for each CatWISE object.

We then binned the matching sources in 0.5 mag bins and computed the standard deviation between the CatWISE and *Gaia* position and motion (shown by the red points in Figure 7–10), as well as the median CatWISE motion uncertainties. For the position analysis, we used the *Gaia* positions moved at the epoch of the CatWISE measurements in the catalog).

We define ten metrics to characterize the astrometric performance of CatWISE:

- σ_{\min} and $\sigma_{\mu, \min}$ are the precision floor for positions and motions, respectively. These precision floors are determined as the median dispersion with respect to *Gaia* in the $8 < W1, W2 < 10$ mag interval, except at low Galactic latitude ($|b| < 10^{\circ}$) where we restrict to the $8 < W1, W2 < 9$ mag since the astrometric precision starts deteriorating significantly beyond $W1, W2 \sim 9$ mag (see e.g. Figure 7–9).
- $W1_{\min}$, $W2_{\min}$, $W1_{\mu, \min}$, and $W2_{\mu, \min}$ are the $W1$ and $W2$ mag at which σ_{\min} and $\sigma_{\mu, \min}$ are exceeded by no more than 20 mas and 5 mas yr $^{-1}$, respectively.
- $W1_{500}$ and $W2_{500}$ are the $W1$ and $W2$ mag at which the precision on coordinates reaches 500 mas.
- $W1_{\mu, 100}$ and $W2_{\mu, 100}$ are the $W1$ and $W2$ mag at which the precision on motion reaches 100 mas yr $^{-1}$.

The results for a subset of 7 representative tiles out of the 141 chosen as test sample are summarized in Table 3 , while in Figure 11 and 12 we plot the results for the full test sample as a function of b and β respectively. We omit the results as a function of source density since all reported metrics do not show clear dependence on it.

σ_{\min} and $\sigma_{\mu, \min}$ are encouragingly small, on the order of 40 mas and 7 mas yr $^{-1}$, respectively. There is little dependence of both metrics on $|b|$ until $|b| < 5$, where they sharply rise towards their peak values of ~ 580 mas and ~ 22 mas yr $^{-1}$.

The plots of $W1_{\min}$, $W2_{\min}$, $W1_{\mu, \min}$, and $W2_{\mu, \min}$ shows strong dependence on $|b|$, with accelerating rise in brightness at lower $|b|$. At high $|b|$ $W1_{\min}$ and $W2_{\min}$ are ~ 13 mag, while $W1_{\mu, \min}$ and $W2_{\mu, \min}$ are ~ 13.5 mag. All metrics rise to ~ 8 mag near the Galactic center.

$W1_{500}$, $W2_{500}$, $W1_{\mu, 100}$ and $W2_{\mu, 100}$ are ~ 17 mag down to $|b| = 20$. For tiles at lower b most $W1_{\mu, 100}$ and $W2_{\mu, 100}$ measurements are upper limits only (open triangles). This is a consequence of the fact that at lower $|b|$ CatWISE only detects brighter sources because of confusion noise, and the motion uncertainties never reach the 100 mas yr $^{-1}$ level. These metrics show a slight dependence on ecliptic latitude, as expected given the deeper coverage at high β .

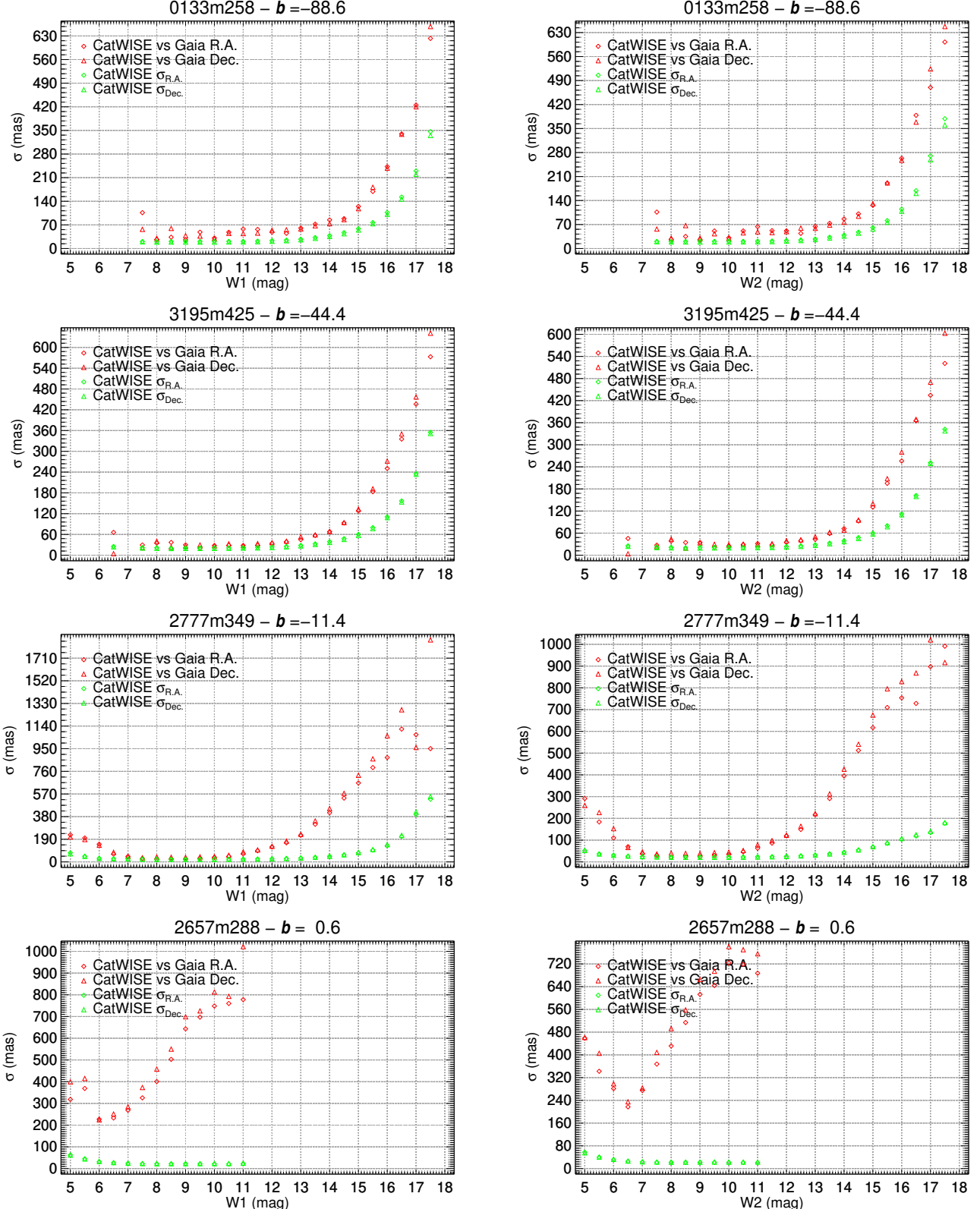


Figure 7. Comparison of CatWISE astrometry against *Gaia* DR2 in four tiles spanning the southern Galactic hemisphere, from the Galactic South Pole (tile 0133m258, top panels) to the Galactic Center (tile 2657m288, bottom panels). The standard deviation between CatWISE position measurements and *Gaia* DR2 position measurements, in 0.5 mag bins, is shown in red. Green points are the median CatWISE uncertainties in the same 0.5 mag bins.

Table 2. CatWISE Astrometric Performance Fields

Tile	<i>l</i>	<i>b</i>	β	Exp	#	Comment
0133m258	139.6	-88.6	-28.8	106	61294	SGP
0890m667	276.5	-30.2	-89.6	7154	71462	SEP
1497p015	237.3	41.4	-10.2	90	58961	COSMOS
2657m288	-0.2	0.6	-5.4	86	63368	GC
2709p666	96.4	29.5	89.6	7839	61702	NEP
2777m349	-0.6	-11.4	-11.6	81	58911	
3195m425	-1.2	-44.4	-25.4	99	57928	

Table 3. CatWISE Astrometric Performance

Tile	Coordinates					Motion				
	σ_{\min}	W1 _{min}	W1 ₅₀₀	W2 _{min}	W2 ₅₀₀	$\sigma_{\mu, \min}$	W1 _{μ, \min}	W1 _{$\mu, 100$}	W2 _{μ, \min}	W2 _{$\mu, 100$}
	mas	mag	mag	mag	mag	mas yr ⁻¹	mag	mag	mag	mag
0133m258	31.9	12.5	17.2	12.5	17.0	7.5	13.5	16.9	13.5	16.7
0890m667	52.9	11.0	15.1	11.0	15.0	7.4	14.5	18.2	14.5	>20.5
1497p015	27.3	12.5	17.0	12.5	16.8	8.5	13.5	16.8	13.5	16.7
2657m288	526.4	8.0	8.4	8.0	8.3	22.2	9.0	>11.0	9.0	>11.5
2709p666	37.7	12.0	18.5	12.0	19.0	7.3	15.5	>19.0	15.5	>20.0
2777m349	32.1	10.5	14.3	10.5	14.4	7.0	12.0	15.9	12.0	15.8
3195m425	27.8	12.5	17.2	13.0	17.2	6.5	13.5	16.9	13.5	16.8

5. SCIENCE

TO BE SUPPLIED

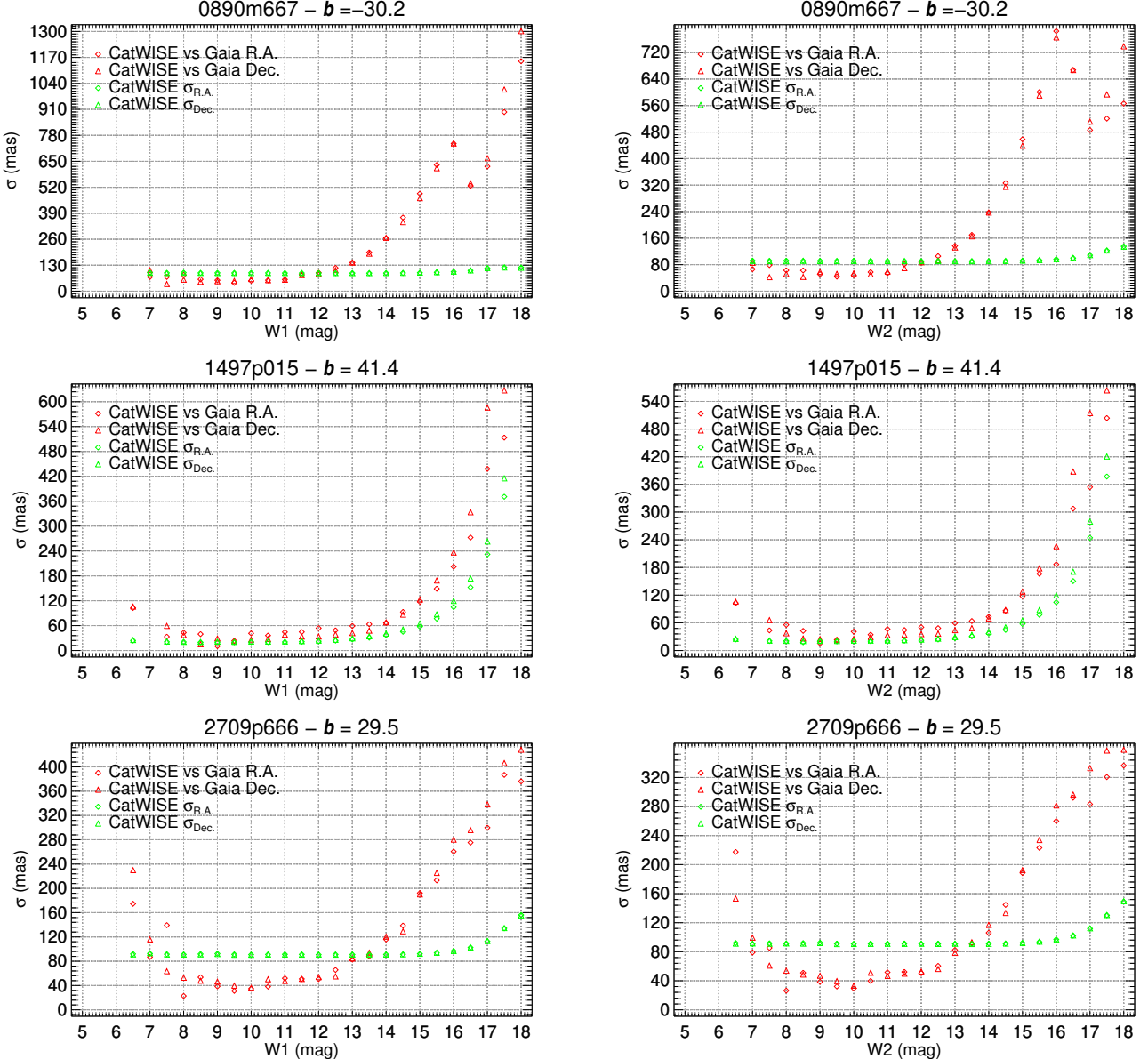


Figure 8. Same as Figure 7, but for the tile containing the South Ecliptic Pole (0890m667), COSMOS (1497p015), and the North Ecliptic Pole (2709p666).

6. DATA ACCESS

Current information about CatWISE data products is provided at <https://catwise.github.io>. The CatWISE catalog and reject files have been transferred to a data repository at the National Energy Research Scientific Computing Center (NERSC). The files were also transferred to the Infrared Science Archive (IRSA), where the individual tile files were merged into the IRSA database.

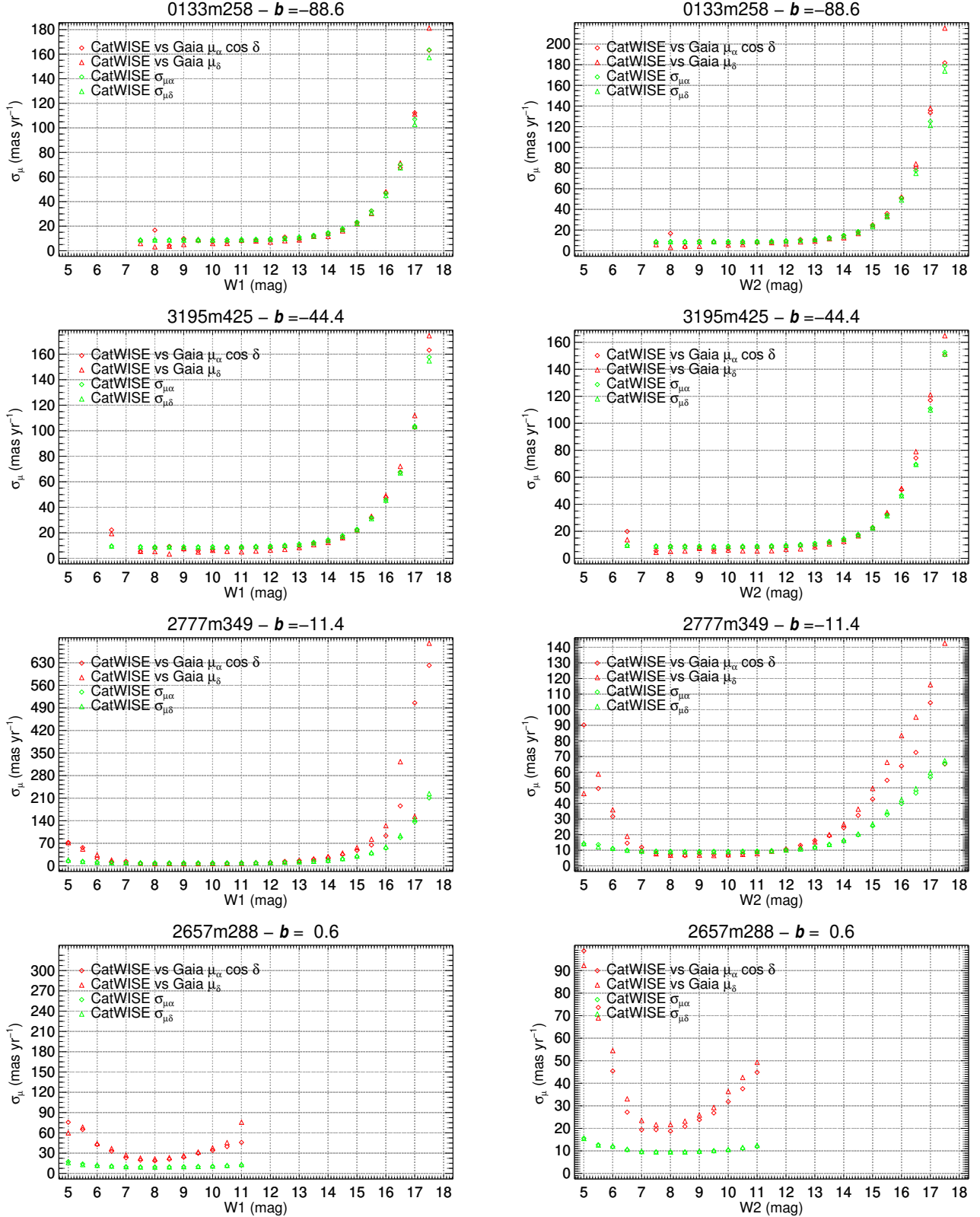


Figure 9. Same as Figure 7, but for motion measurements.

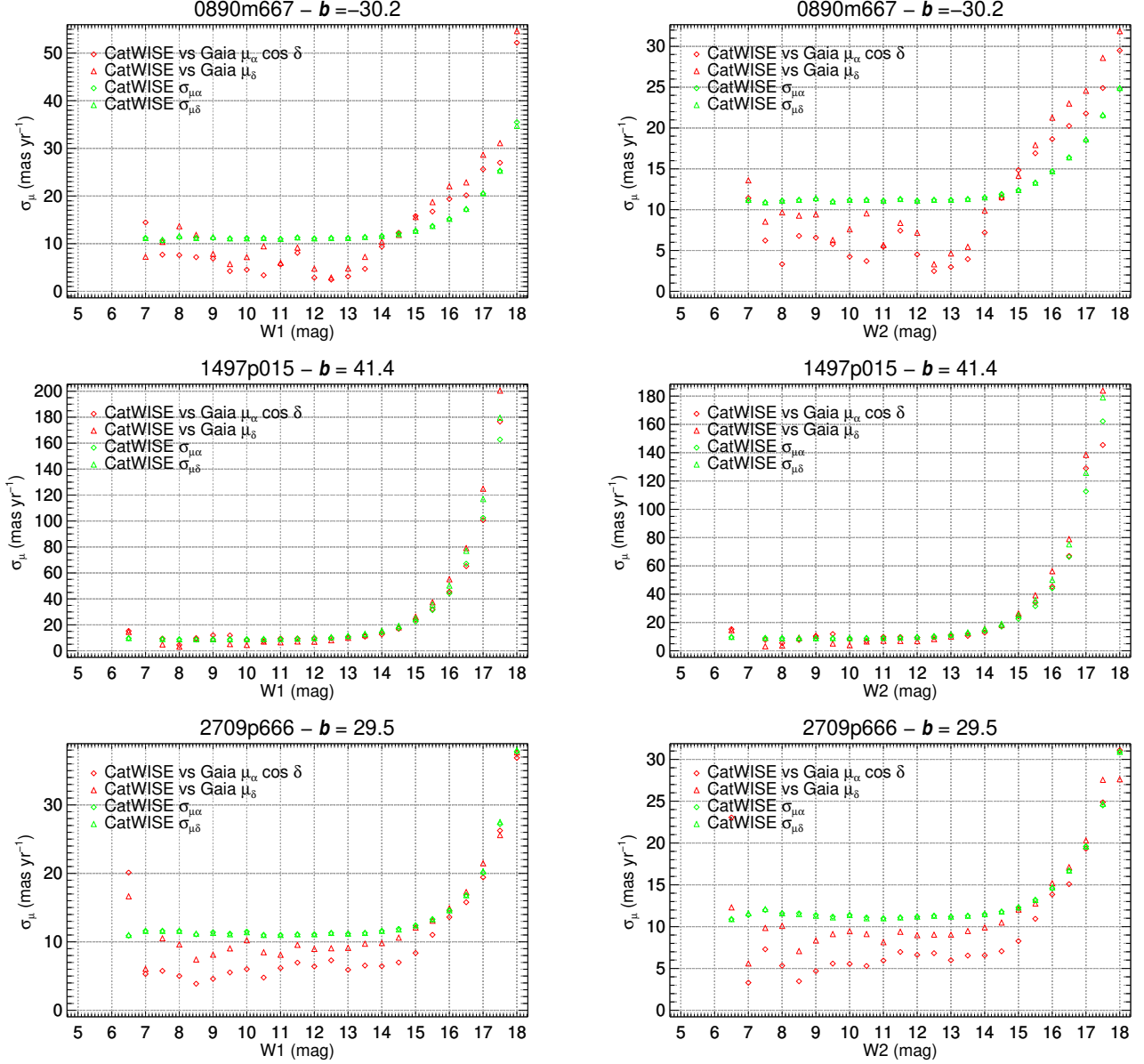


Figure 10. Same as Figure 9, but for the tile containing the South Ecliptic Pole (0890m667), COSMOS (1497p015), and the North Ecliptic Pole (2709p666).

The Preliminary CatWISE catalog is accessible at

<https://portal.nersc.gov/project/cosmo/data/CatWISE/prelim>

in 18,240 pairs of gzipped ascii files (one catalog and one reject file per tile) in IPAC table format, organized into 359 directories, one for each decimal degree of right ascension from 0 to 358 (there are no tiles beginning with 359). Text files providing the format and a brief description of the columns

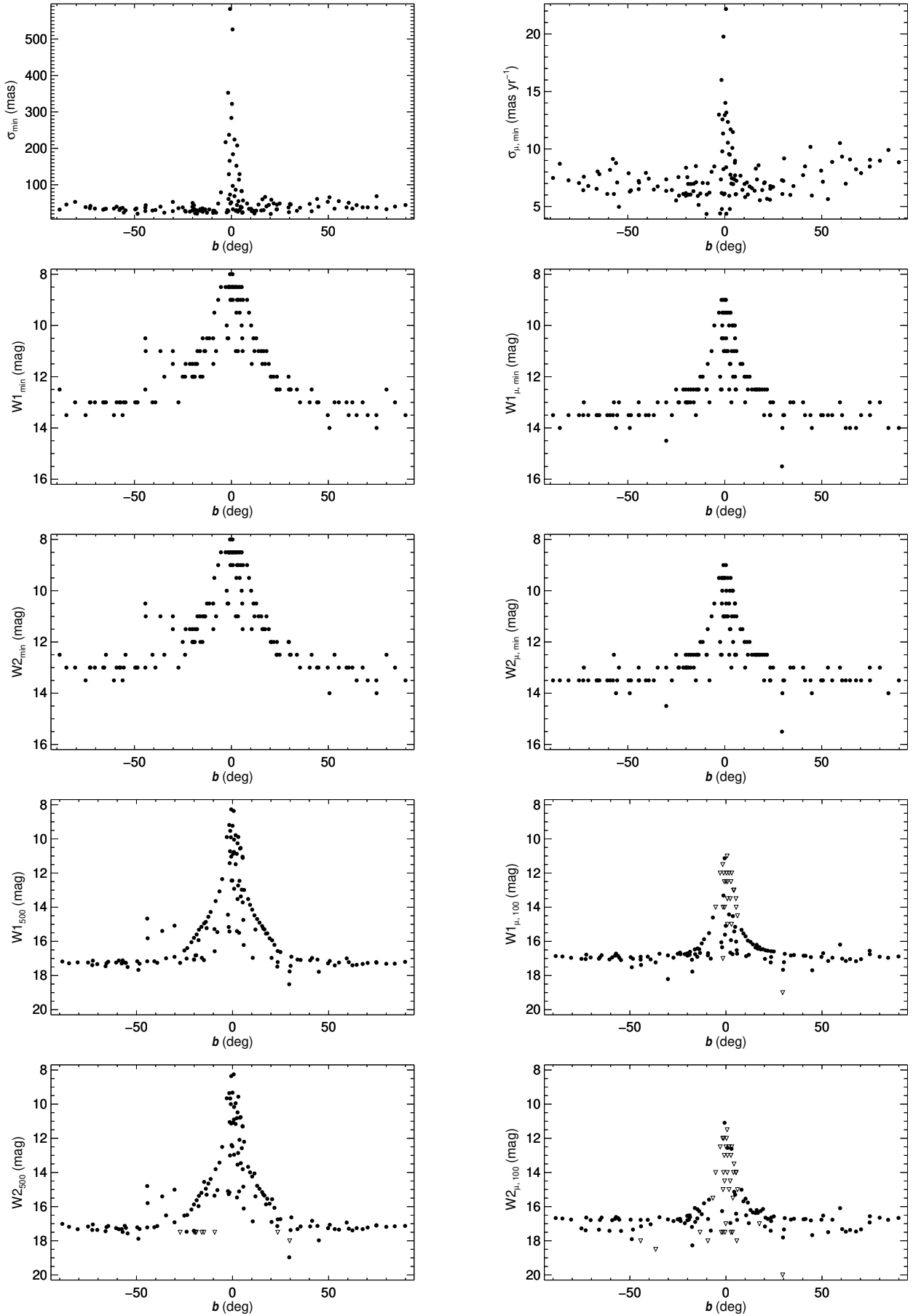


Figure 11. Astrometric performance of CatWISE as a function of Galactic latitude

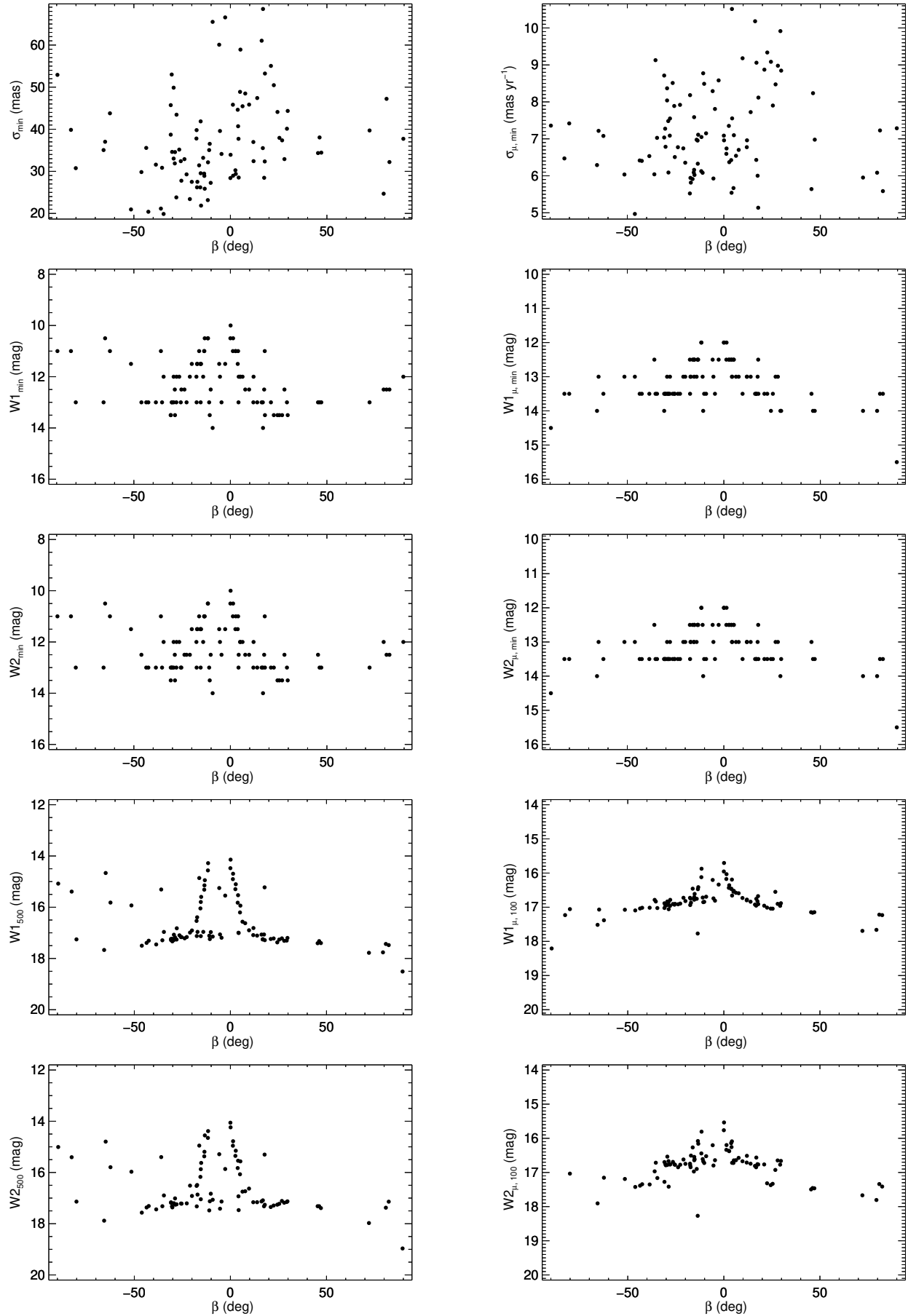


Figure 12. Astrometric performance of CatWISE as a function of Ecliptic latitude

in the catalog and reject files are provided there. The Preliminary catalog will also soon become available from IRSA (<https://irsa.ipac.caltech.edu>) as a contributed data set.

CatWISE uses data products from WISE, which is a joint project of the University of California, Los Angeles, and the Jet Propulsion Laboratory (JPL)/California Institute of Technology (Caltech), funded by the National Aeronautics and Space Administration (NASA), and from NEOWISE, which is a JPL/Caltech project funded by NASA. Characterization of CatWISE performance uses data from Gaia and from Spitzer. CatWISE is led by JPL/Caltech, with funding from NASA’s Astrophysics Data Analysis Program (ADAP), and is also supported in part by ADAP grant NNH17AE75I at Lawrence Berkeley Laboratory. CatWISE is also supported by the Fellowships and Internships in Extremely Large Data Sets (FIELDS) program funded by NASA at UC Riverside. FM is supported by an appointment to the NASA Postdoctoral Program at the Jet Propulsion Laboratory, administered by Universities Space Research Association under a contract with NASA.

APPENDIX

A. COMBINING ASCENDING AND DESCENDING SCAN POSITIONS

Here we provide additional details on how ascending and descending scan positions are combined for the Preliminary CatWISE catalog. Positions are averaged using inverse-covariance weighting. The averaging is done in a local Cartesian projection consistent with the uncertainty representation.

A transformation matrix (T) is defined as follows: starting with a Cartesian XYZ system whose Z axis points to the celestial north pole and whose X axis points to the vernal equinox, we perform two Euler rotations that place the new Z axis on the ascending celestial (α, δ) position with the Y axis aligned with the local north-south direction, and the X axis aligned with the local east-west direction. This corresponds to a Z axis that looks outward from the origin, so any nearby α', δ' position will have a celestial $X'Y'Z'$ vector whose Z' coordinates will be positive and close to 1. By “nearby” we mean within a few arcseconds of the origin, since it is very rare for an extracted source’s position to

vary between the ascending and descending solutions by more than that. This justifies our Cartesian approximation.

The coordinate system is computed for the ascending position, so that the ascending position of the source is $X = 0, Y = 0$. The descending position (α', δ') is mapped into that system as follows. We construct the vector to the descending position in the original celestial coordinate system and transform it into the new system, wherein its X and Y offsets from the origin correspond to (α, δ) offsets of the descending position from the ascending position.

The offset vector is averaged with $(0,0)$ using inverse covariance weighting. We construct 2×2 error covariance matrices Ω_a and Ω_d for the ascending and descending vectors using the corresponding σ_α , σ_δ , and $\sigma_{\alpha\delta}$:

$$\begin{aligned}\Omega_a &= \begin{bmatrix} \sigma_\alpha^2 & \sigma_{\alpha\delta} |\sigma_{\alpha\delta}| \\ \sigma_{\alpha\delta} |\sigma_{\alpha\delta}| & \sigma_\delta^2 \end{bmatrix}_a \\ \Omega_d &= \begin{bmatrix} \sigma_\alpha^2 & \sigma_{\alpha\delta} |\sigma_{\alpha\delta}| \\ \sigma_{\alpha\delta} |\sigma_{\alpha\delta}| & \sigma_\delta^2 \end{bmatrix}_d\end{aligned}\tag{A1}$$

A minimum value of 0.0001 is enforced for any zeroes on the diagonal. The merged (i.e., inverse-covariance-weighted average) vector $(X_m Y_m Z_m)$ and merged covariance matrix are computed as follows:

$$W_a = \Omega_a^{-1}, \quad W_d = \Omega_d^{-1}\tag{A2}$$

$$\Omega = (W_a + W_d)^{-1} \equiv \begin{bmatrix} \Omega_{11} & \Omega_{12} \\ \Omega_{21} & \Omega_{22} \end{bmatrix}\tag{A3}$$

$$\begin{bmatrix} X_m \\ Y_m \end{bmatrix} = \Omega \left(W_a \begin{bmatrix} 0 \\ 0 \end{bmatrix}_a + W_d \begin{bmatrix} X' \\ Y' \end{bmatrix}_d \right) = \Omega W_d \begin{bmatrix} X' \\ Y' \end{bmatrix}_d$$

$$Z_m = \sqrt{1 - X_m^2 - Y_m^2}$$
(A4)

$$\sigma_\alpha = \sqrt{\Omega_{11}}, \quad \sigma_\delta = \sqrt{\Omega_{22}}, \quad \sigma_{\alpha\delta} = \text{sign}(\Omega_{12}) \sqrt{|\Omega_{12}|}$$
(A5)

The celestial coordinates corresponding to the $X_m Y_m Z_m$ vector are obtained using the inverse of the transformation matrix (T) described above (the inverse in the transpose because T is orthonormal):

$$\begin{bmatrix} V'_1 \\ V'_2 \\ V'_3 \end{bmatrix} \equiv \begin{bmatrix} T_{11} & T_{21} & T_{31} \\ T_{12} & T_{22} & T_{32} \\ T_{13} & T_{23} & T_{33} \end{bmatrix} \begin{bmatrix} X_m \\ Y_m \\ Z_m \end{bmatrix}$$
(A6)

$$\alpha_m = \tan^{-1} \left(\frac{V'_2}{V'_1} \right), \quad \delta_m = \sin^{-1} V'_3$$
(A7)

The image pixel coordinates are then computed for the merged position using the coadd WCS information.

REFERENCES

- Caselden, D., Westin, P., Meisner, A., et al. 2018,
ASCL:1806.004.
- Connors, M., Wiegert, P., & Veillet, C. 2011,
Nature, 475, 481
- Cutri, R. M., Wright, E. L., Conrow, T., et al.
2013, Explanatory Supplement to the AllWISE
Data Release Products,
<http://wise2.ipac.caltech.edu/docs/release/allwise/expsup>
- Cutri, R. M., Mainzer, A., Conrow, T., et al.
2015, Explanatory Supplement to the
NEOWISE Data Release Products,
<http://wise2.ipac.caltech.edu/docs/release/neowise/expsup>
- Cutri, R. M., Wright, E. L., Conrow, T., et al.
2012, Explanatory Supplement to the WISE
All-Sky Data Release Products,
<http://wise2.ipac.caltech.edu/docs/release/allsky/expsup>

- Gaia Collaboration, Brown, A. G. A., Vallenari, A., et al. 2018, *A&A*, 616, A1
- Jarrett, T. H., Cohen, M., Masci, F., et al. 2011, *ApJ*, 735, 112
- Kirkpatrick, J. D., Schneider, A., Fajardo-Acosta, S., et al. 2014, *ApJ*, 783, 122
- Lang, D. 2014, *AJ*, 147, 108
- Lindgren, L., Hernández, J., Bombrun, A., et al. 2018, *A&A*, 616, A2
- Luhman, K. L. 2013, *ApJL*, 767, L1
- Luhman, K. L. 2014, *ApJL*, 786, L18
- Marsh, K. A., & Jarrett, T. H. 2012, *PASA*, 29, 269
- Masci, F. 2013, arXiv:1301.2718
- Mainzer, A., Bauer, J., Grav, T., et al. 2011, *ApJ*, 731, 53
- Mainzer, A., Bauer, J., Cutri, R. M., et al. 2014, *ApJ*, 792, 30
- Mainzer, A., Bauer, J., Cutri, R. M., et al. 2014, *ApJ*, 792, 30
- Mauduit, J.-C. Lacy, M. Farrah, D., et al. 2012, *PASP*, 124, 714
- Meisner, A. M., Lang, D., & Schlegel, D. J. 2018a, *AJ*, 156, 69
- Meisner, A. M., Cushing, M. C., Cutri, R., et al. 2018b, *RNAAS*, 2, 1
- Meisner, A. M., Cushing, M. C., Cutri, R., et al. 2018c, *RNAAS*, 2, 140
- Meisner, A. M., Lang, D., & Schlegel, D. J. 2018d, *RNAAS*, 2, 202
- Sanders, D. B., Salvato, M., Aussel, H., et al. 2007, *ApJS*, 172, 86
- Schlafly, E. F., Meisner, A. M., & Green, G. M. 2019, *ApJS*, 240, 30
- Scholz, R.-D. 2014, *A&A*, 561, A113
- Tsai, C.-W., Eisenhardt, P. R. M., Wu, J., et al. 2015, *ApJ*, 805, 90
- Wright, E. L., Eisenhardt, P. R. M., Mainzer, A. K., et al. 2010, *AJ*, 140, 1868